

Elastic scattering of ${}^7\text{Li}+{}^{58}\text{Ni}$: a phenomenological and microscopic analysis

Norah A.M. Alsaif

Department of Physics, College of Science, Princess Nourah bint Abdulrahman University, Riyadh, Saudi Arabia.

Sh. Hamada

Faculty of Science, Tanta University, Tanta, Egypt.

M. El-Azab Farid

Physics Department, Assiut University, Assiut, 71516, Egypt.

B.M. Alotaibi

Department of Physics, College of Science, Princess Nourah bint Abdulrahman University, Riyadh, Saudi Arabia.

Mohammed Alotiby

*Nuclear Technologies Institute (NTI), King Abdulaziz City for Science & Technology (KACST),
P. O. Box 6086, Riyadh, 11442, Saudi Arabia.*

Awad A. Ibraheem

*Physics Department, King Khalid University, Abha, Saudi Arabia,
Physics Department, Al-Azhar University, Assiut Branch, Assiut 71524, Egypt.*

Received 27 April 2022; accepted 9 June 2022

Motivating by examining the break-up effect of ${}^7\text{Li}$ projectile into $t+\alpha$ cluster structure in the field of ${}^{58}\text{Ni}$ nucleus, the available experimental angular distributions for ${}^7\text{Li} + {}^{58}\text{Ni}$ elastic scattering system at energies ranging from 13 and up to 42 MeV are studied utilizing different phenomenological as well as microscopic potentials. Data analysis utilizing the Sao Paulo potential revealed that in order to reproduce the data, the strength of the real folded potential had to be reduced by $\sim 36\%$. While, data analysis utilizing the double folding CDM3Y6 potential with and without the rearrangement term revealed that the potential strength needed to be reduced by ~ 63 and 62% , respectively. Cluster folding model based on the $t + \alpha$ cluster structure for ${}^7\text{Li}$ is applied to reproduce the considered data. Similar results were obtained showing the necessity to reduce real cluster folding potential strength by about 49% . The reported reduction in potential strength from the different implemented potentials supports the strong ${}^7\text{Li}$ break-up impact. Finally, the full microscopic continuum discretized coupled channels approach is applied with a great success in reproducing the considered data.

Keywords: Elastic scattering; optical potential; folding potential; cluster folding model; Sao Paulo potential; CDCC method.

DOI: <https://doi.org/10.31349/RevMexFis.69.021201>

1. Introduction

Nuclear processes involve loosely projectiles such as ${}^6,{}^7\text{Li}$ and ${}^9,{}^{10},{}^{11}\text{Be}$ is a hot research topic that attracts nuclear physicists for decades due to their high clusterization probability. This study is devoted to investigate the mechanism of interaction of the weakly bound ${}^7\text{Li}$ ions in the field of a medium mass target – ${}^{58}\text{Ni}$ – at energies ranges from 13 MeV (below the Coulomb barrier energy, E_C) and up to 42 MeV. In connection with this aim, the available ${}^7\text{Li} + {}^{58}\text{Ni}$ experimental angular distributions (ADs) measurements are reanalyzed from both the phenomenological and the microscopic point of view.

There are many experimental [1-6] and theoretical [7-13] studies for ${}^7\text{Li} + {}^{58}\text{Ni}$ nuclear system. In Ref. [1], the ${}^7\text{Li} + {}^{58}\text{Ni}$ elastic scattering ADs at five different energies (12.0, 12.5, 13.0, 13.5 and 14.22 MeV) around the Coulomb barrier were experimentally measured. The measured data were analyzed using the double-folding (DF) Sao Paulo potential (SPP) for the real part as well as an imagi-

nary Woods-Saxon (WS) potential. Pfeiffer *et al.* [2] investigated the break-up effect of ${}^6,{}^7\text{Li}$ on ${}^{58}\text{Ni}$ and ${}^{118}\text{Sn}$ targets at energies 12 – 24 MeV showing that, both the total and the differential cross sections (DCs) could be predicted as a function of the bombarding energy relative to E_C . Elastic ADs for ${}^7\text{Li}$ scattered from ${}^{58,60}\text{Ni}$, ${}^{56}\text{Fe}$ and ${}^{44}\text{Ca}$ at $E_{\text{lab}} = 34$ MeV were measured by Glover *et al.* [4]. The measured data were reproduced by the phenomenological optical model (OM) using real and imaginary volume WS potentials, as well as using a double-folding real potential multiplied by approximately 0.6. In Ref. [5], the ADs of the elastic and break-up cross sections for ${}^7\text{Li}$ ions beam scattered from ${}^{58}\text{Ni}$ target at $E_{\text{lab}} = 42$ MeV were measured. The significant ${}^7\text{Li}$ break-up contributions were found to come from the decay of the $(7/2^-, E_x = 4.63$ MeV) resonant state of ${}^7\text{Li}$ with some indications of other contributions from the $(5/2^-, E_x = 6.68$ MeV and $5/2^-, E_x = 7.46$ MeV) states. Zevra *et al.* [6] determined the barrier distributions for ${}^6,{}^7\text{Li}$ elastically scattered from ${}^{58}\text{Ni}$, ${}^{116,120}\text{Sn}$ and ${}^{208}\text{Pb}$ targets at sub- and near-barrier energies as well as excitation functions at

$\pm 160^\circ$, and $\pm 170^\circ$, for probing the potential at near barrier energies and the pertinent reaction mechanisms.

In addition to the previously experimental measurements, different theoretical studies [7-13] were devoted to investigate ${}^7\text{Li} + {}^{58}\text{Ni}$ system. In Ref. [7], the elastic scattering ADs for ${}^7\text{Li}$ ions of energies below 450 MeV scattered on different targets ${}^{27}\text{Al}$ to ${}^{208}\text{Pb}$ were calculated by the ${}^7\text{Li}$ microscopic optical potential (MOP) based on the Skyrme nucleon-nucleon effective interaction. Reasonable agreement with the experimental data was obtained but with some discrepancies observed at relatively larger angles. The analysis showed that the MOP could be enhanced by introducing a repulsive potential to the real part and an absorptive potential to the imaginary part which could be achieved by considering the ${}^7\text{Li}$ break-up effect. In Ref. [9] Basak *et al.*, analyzed the elastic scattering cross-sections and vector analyzing powers for ${}^{6,7}\text{Li}$ ions scattered on different targets: ${}^{12}\text{C}$, ${}^{26}\text{Mg}$, ${}^{58}\text{Ni}$ and ${}^{120}\text{Sn}$ nuclei using OM potential with a real double folded part with a reasonable success. This investigation showed the success of the simple OM analysis to account well for the opposite signs of the vector analyzing power data for ${}^{6,7}\text{Li} + {}^{120}\text{Sn}$ at $E_{\text{lab}} = 44$ MeV and for ${}^{6,7}\text{Li} + {}^{58}\text{Ni}$ at $E_{\text{lab}} \approx 20$ MeV. In Ref. [10], The elastic and inelastic ADs for ${}^{6,7}\text{Li}$ scattered from ${}^{12}\text{C}$, ${}^{28}\text{Si}$ and ${}^{58}\text{Ni}$ targets in the energy range 12 – 35 MeV/u were analyzed using coupled-channels (CC) method with potentials constructed using the S1Y effective nucleon-nucleon interaction. Using the adopted technique, successful description of the data was obtained.

This work complements our previous studies [14-19] devoted for studying the peculiarities and the interaction mechanisms of weakly projectiles with different target nuclei at energies both below and above the E_C . The paper is structured as follows. Sec. 2 presents the implemented potentials in the theoretical calculations. Section 3 presents the results of data analysis and discussion. Section 4 is devoted to the summary.

2. Implemented potentials in theoretical calculations

The considered ${}^7\text{Li} + {}^{58}\text{Ni}$ elastic scattering ADs at energies 13 – 42 MeV are reanalyzed utilizing different approaches and potentials starting from the simplest one (OM) through the microscopic approaches such as double folding CDM3Y6 and SPP potentials, and ending with the most sophisticated and full microscopic continuum discretized coupled channels (CDCC) method which is applied with a great success in reproducing the considered data. The analysis in such way could clarify the different characterizations of ${}^7\text{Li} + {}^{58}\text{Ni}$ system as well as helps in obtaining the optimal potentials that fairly reproduce the considered experimental data. The cluster folding model (CFM) based on the t and α + target potential is used to consider the $t + \alpha$ cluster structure of ${}^7\text{Li}$.

2.1. The analysis using optical model

As a first step, the experimental elastic scattering ${}^7\text{Li} + {}^{58}\text{Ni}$ ADs at energies of 13 and 13.5 MeV [1], 14.22, 16.25, 18.28, and 20.31 MeV [2], 19 MeV [3], 34 MeV [4], and 42 MeV [5] are reanalyzed using the phenomenological OM with a central potential which has the following form: ear systems, OM of the nucleus is applied. The implemented phenomenological OM potential has the following form:

$$U(r) = V_C - V_0 \left[1 + \exp\left(\frac{r - R_V}{a_V}\right) \right]^{-1} - iW_0 \left[1 + \exp\left(\frac{r - R_W}{a_W}\right) \right]^{-1}. \quad (1)$$

The first term $V_C(r)$ is the Coulomb potential due to a uniform sphere with a charge equal to that of the target nucleus and radius $r_C A_t^{1/3}$.

The second and third terms are the real and imaginary parts of nuclear potential which describe the scattering and absorption processes, respectively. Both parts are of volume shape and expressed in the conventional WS form. The spin orbit potential (V_{SO}) for ${}^7\text{Li}$ has been excluded as it has a little effect as well as for the sake of simplicity.

2.2. The analysis using Sao Paulo potential

It is more preferable to construct the interaction potential using more microscopic methods in order to get rid of the different ambiguities inherited with the OM potential. The SPP is similar to the usual DF potential as it is based on folding the projectile and target densities with nucleon-nucleon interaction potential (V_{NN}) [20-24] expressed as.

$$V_{DF}(r) = \iint \rho_p(r_1) \rho_t(r_2) v_0 \delta(|\vec{S}|) d^3r_1 d^3r_2, \quad (2)$$

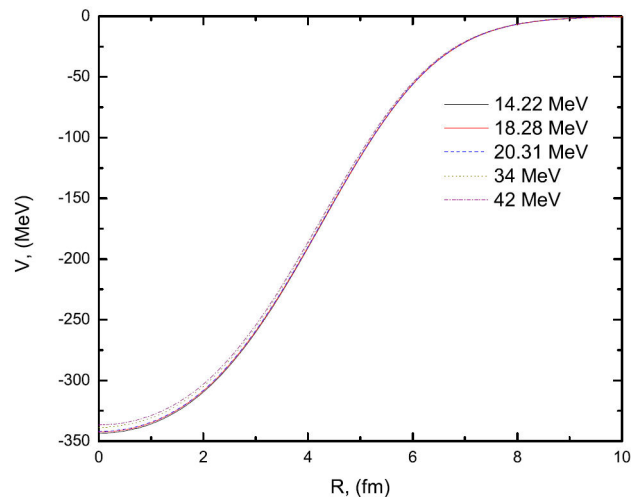


FIGURE 1. The generated real SPP at energies $E_{\text{lab}} = 14.22, 18.28, 20.31, 34,$ and 42 MeV.

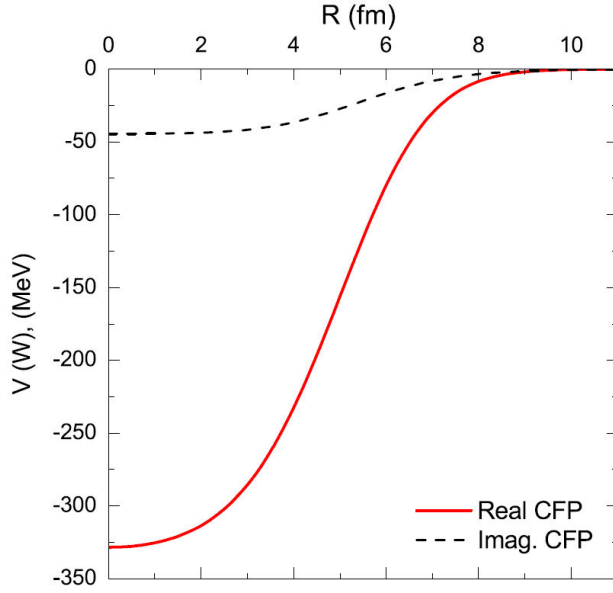


FIGURE 2. The implemented real and imaginary CFPs in the ${}^7\text{Li} + {}^{58}\text{Ni}$ CFM analysis.

where the density distributions of ${}^7\text{Li}$ and ${}^{58}\text{Ni}$ nuclei are denoted by $\rho_p(r_1)$ and $\rho_t(r_2)$, respectively. The nuclear densities for ${}^7\text{Li}$ and ${}^{58}\text{Ni}$ were taken from the tabulated values created by REGINA code and were prepared based on the Dirac-Hartree-Bogoliubov (DHB) model [25]. The prepared SPP at $E_{\text{lab}} = 14.22, 18.28, 20.31, 34,$ and 42 MeV are shown in Fig. 1.

2.3. The analysis using cluster folding model

Due to the well-developed $\alpha + t$ cluster structure in ${}^7\text{Li}$ nucleus that appears at $E_x = 2.468$ MeV, various break-up effects are observed in different system induced by this weakly bound projectile. Better understanding the dissociation nature of ${}^7\text{Li}$ would clarify the dissociation of loosely unstable radioactive isotopes. The resulted break-up of ${}^7\text{Li}$ into a triton (valence particle) orbiting an α -particle (core) can have a significant effect even on elastic scattering data. In order to check this effect, it is desirable to derive the ${}^7\text{Li} + {}^{58}\text{Ni}$ nuclear interaction potential based on a microscopic method that considers the ${}^7\text{Li}$ cluster nature, such as the fully microscopic cluster folding model (CFM). In the CFM, the real and imaginary cluster folding potentials (CFPs) for the ${}^7\text{Li} + {}^{58}\text{Ni}$ system are generated based on the $t + {}^{58}\text{Ni}$ and $\alpha + {}^{58}\text{Ni}$ potentials as follows:

$$V^{CF}(\mathbf{R}) = \int \left[V_{\alpha-{}^{58}\text{Ni}} \left(\mathbf{R} - \frac{3}{7}\mathbf{r} \right) + V_{t-{}^{58}\text{Ni}} \left(\mathbf{R} + \frac{4}{7}\mathbf{r} \right) \right] |\chi_{\alpha-t}(\mathbf{r})|^2 d\mathbf{r}, \quad (3)$$

$$W^{CF}(\mathbf{R}) = \int \left[W_{\alpha-{}^{58}\text{Ni}} \left(\mathbf{R} - \frac{3}{7}\mathbf{r} \right) + W_{t-{}^{58}\text{Ni}} \left(\mathbf{R} + \frac{4}{7}\mathbf{r} \right) \right] |\chi_{\alpha-t}(\mathbf{r})|^2 d\mathbf{r}. \quad (4)$$

The suitable needed potentials are: $V_{t-{}^{58}\text{Ni}}$ at $E_{\text{lab}} = 18$ MeV ($E_t \approx 3/7 E_{Li}$) and $V_{\alpha-{}^{58}\text{Ni}}$ at $E_{\text{lab}} = 24$ MeV ($E_\alpha \approx 4/7 E_{Li}$). As the ${}^7\text{Li} + {}^{58}\text{Ni}$ AD data at 42 MeV is the greatest regarded energy, the $t + {}^{58}\text{Ni}$ at $E_{\text{lab}} = 17$ MeV [26] and $\alpha + {}^{58}\text{Ni}$ at $E_{\text{lab}} = 24.1$ MeV [27] are the most appropriate data for determining the CFPs for ${}^7\text{Li} + {}^{58}\text{Ni}$ based on prior investigations regarding t and α scattered from ${}^{58}\text{Ni}$ target. In the ground state of ${}^7\text{Li}$, the $\chi_{\alpha-t}(\mathbf{r})$ is the inter-cluster wave function that characterizes the relative motion of α and t . The $\alpha - t$ bound state form factor represents a $2P_{3/2}$ state in a real WS potential with a radius of 1.83 fm, a diffuseness of 0.65 fm, and a depth that can change until the cluster's binding energy (2.468 MeV) is reached. The created CFPs are shown in Fig. 2, these potentials well agree with the previously created CFPs by Nishioka *et al.*, [13].

3. Results and discussion

3.1. Analysis of ${}^7\text{Li} + {}^{58}\text{Ni}$ data using OM potential

The elastic scattering ADs for ${}^7\text{Li} + {}^{58}\text{Ni}$ system at energies ranging from 13 – 42 MeV [1-5] are reanalyzed phenomenologically using OM of central potential presented in Eq. (1). The implemented OM potential consists of a Coulomb part of radius $1.4 \times (58)^{1/3}$ in addition to nuclear part. The calculations were performed using fixed geometry parameters to observe how the real and imaginary potential depths vary with bombarding energy. In accordance with Cook study [28]

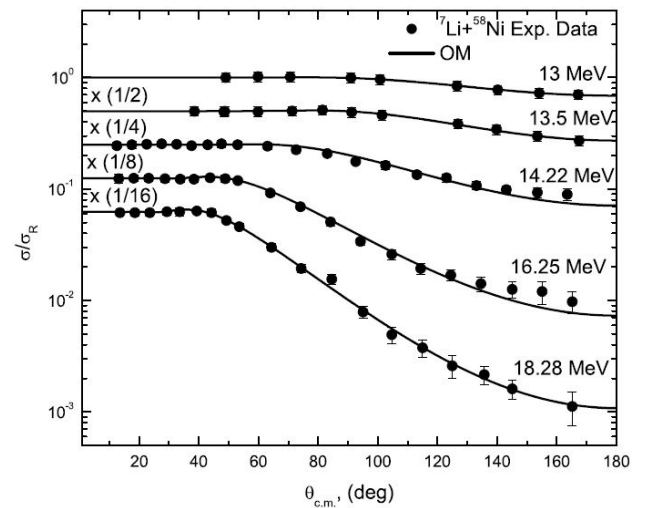


FIGURE 3. Comparison between ${}^{58}\text{Ni}({}^7\text{Li}, {}^7\text{Li}){}^{58}\text{Ni}$ elastic scattering ADs (circles) and OM fits (curves) at $E_{\text{lab}} = 13, 13.5, 14.22, 16.25,$ and 18.28 MeV.

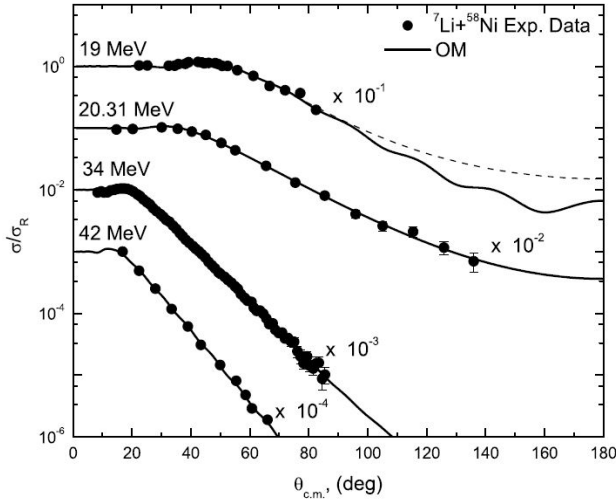


FIGURE 4. Same as Fig. 3 but at $E_{lab} = 19, 20.31, 34,$ and 42 MeV. The dashed line refers to OM fit using another potential set which is applied to wash up the observed oscillations at $E = 19$ MeV.

concerning the systematic global optical potential for ^7Li projectile, the following parameters $r_V, r_W, a_V,$ and a_W were fixed to 1.286, 1.739, 0.853, and 0.809 fm, respectively. Consequently, two adjustable parameters V_0 (real potential depth) and W_0 (imaginary potential depth) were used to fit the data. The experimental data for $^7\text{Li} + ^{58}\text{Ni}$ ADs at all the considered energies below and above the E_c is fairly reproduced utilizing the OM approach as presented in Figs. 3 and 4 using the extracted parameters displayed in Table I.

In order to check the applicability of the dispersion relation on real (J_V) and imaginary (J_W) volume integrals, these quantities were calculated as their values are displayed in Table I. It is clearly shown that, the extracted (J_V) and (J_W) values don't obey the usual dispersion relation (localized peak followed by a continuous decrease in J_V values, and direct increase followed by nearly constant energy dependence for J_W values). The performed OM analysis gives an evidence for the absence of usual threshold anomaly (TA) which is presented in many systems induced by tightly bounded pro-

jectiles [29-32]. This absence of TA is observed in some systems induced by weakly projectiles [33,34], the so called break-up threshold anomaly (BTA) phenomenon.

The quality of fitting and hence the optimal potential parameters were obtained by minimizing the χ^2 value which defines the deviation between experimental data and calculations, and defined as follow:

$$\chi^2 = \frac{1}{N} \sum_{i=1}^N \left(\frac{\sigma(\theta_i)^{\text{cal}} - \sigma(\theta_i)^{\text{exp}}}{\Delta\sigma(\theta_i)} \right)^2. \quad (5)$$

The $\sigma(\theta_i)^{\text{exp}}$ and $\sigma(\theta_i)^{\text{cal}}$ are the experimental and calculated (DCs), $\Delta\sigma(\theta_i)$ is the relative uncertainty in experimental data. FRESKO code [35] upgraded with χ^2 minimization SFRESKO code were implemented to fit the data and to get the optimal potential parameters. Although the OM calculations using real and imaginary WS potentials were successful in reproducing the considered data, the fitting at $E = 19$ MeV showed some oscillations which are mainly linked to the used potential parameters. In order to wash up these oscillations, we had to reduce the applied constraints by allowing the real and imaginary depth (V_0 and W_0) and diffuseness (a_V and a_W) to freely change till the best fit is reached, and the radius parameters were still fixed ($r_V = 1.286$ fm and $r_W = 1.739$ fm). The used parameters to fit the data at $E = 19$ MeV are: $V_0 = 99.15$ MeV, $a_V = 0.908$ fm, $W_0 = 28.6$ MeV and $a_W = 0.502$ fm, and the obtained fit utilizing such parameters is represented by the dashed line in Fig. 4.

3.2. Analysis of $^7\text{Li} + ^{58}\text{Ni}$ data using SPP

Despite the well-known success of the OM to reproduce the experimental results for a variety of nuclear systems, it is preferable to construct the interaction potential on more microscopic methods such as SPP. This fact arises from the different parameter ambiguities both discrete and continuous associated with OM calculations. In order to overcome these ambiguities and to take the internal structure of the interacting nuclei into consideration, the new version SPP2 [36] was

TABLE I. Optimal OM potential parameters for $^7\text{Li} + ^{58}\text{Ni}$ system with fixed $r_V = 1.286$ fm, $r_W = 1.739$ fm, $a_V = 0.853$, and $a_W = 0.809$ fm. The values of (J_V), (J_W) and reaction cross sections (σ_R) are displayed.

E (MeV)	V_0 (MeV)	W_0 (MeV)	χ^2/N	σ_R (mb)	J_V MeV.fm ³	J_W MeV.fm ³
13	92.93	8.34	0.06	77.41	152.55	29.99
13.5	108.13	6.1	0.02	101.7	177.50	21.93
14.22	90.0	24.95	0.66	347.4	147.74	89.71
16.25	104.09	54.9	0.5	863.7	170.87	197.36
18.28	110.29	52.51	0.23	1128	181.05	188.80
19	99.88	6.17	1.17	720.2	163.96	22.18
20.31	162.13	51.46	0.32	1366	266.15	185.03
34	109.98	24.77	0.56	1804	180.54	89.06
42	73.86	16.98	11.4	1807	121.25	61.05

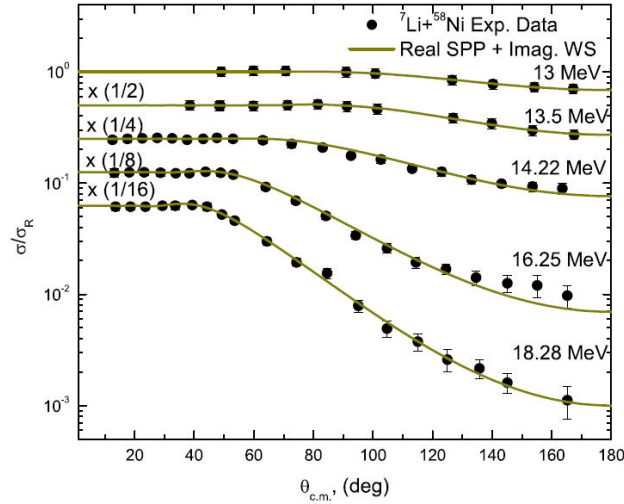


FIGURE 5. Comparison between ${}^{58}\text{Ni}({}^7\text{Li}, {}^7\text{Li}){}^{58}\text{Ni}$ ADs (circles) and calculations using (real SPP + Imag. WS) approach (curves) at $E_{\text{lab}} = 13, 13.5, 14.22, 16.25,$ and 18.28 MeV.

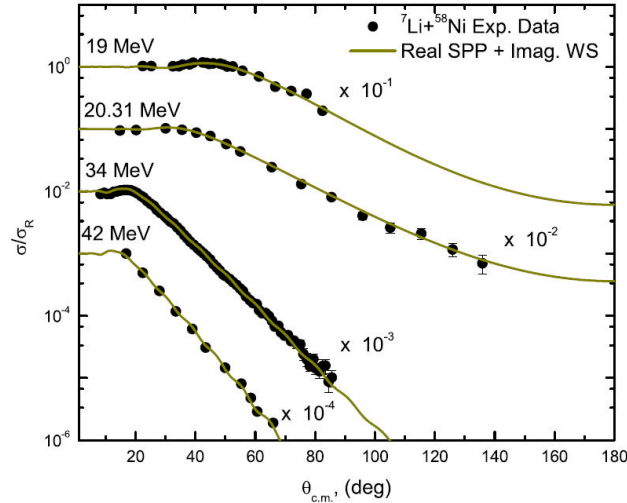


FIGURE 6. Same as Fig. 5 but at $E_{\text{lab}} = 19, 20.31, 34,$ and 42 MeV.

applied to investigate the concerned ${}^7\text{Li} + {}^{58}\text{Ni}$ ADs data. The real part of SPP was created using (Eq. (2)) and the imaginary part was taken of WS shape with potential parameters fixed to their optimal values obtained from OM analysis. The implemented potential has the following shape:

$$U(R) = V_C(R) - N_{RSPP} V^{DF}(R) - iW_0 \left[1 + \exp\left(\frac{r - R_W}{a_W}\right) \right]^{-1}, \quad (6)$$

where N_{RSPP} is the renormalization factor for the real part of the adopted SPP, and its optimal extracted values are displayed in Table II. As shown in Figs. 5 and 6, reasonable agreement was obtained between the experimental ${}^7\text{Li} + {}^{58}\text{Ni}$ ADs and the theoretical calculations utilizing (real SPP + Imag. WS) approach.

Two important facts are presented in the performed analysis. First, an observed reduction in the N_{RSPP} value was found to be necessary for fitting well the data at the different considered energies with an average value 0.64 ± 0.18 . These results show that, in order to reproduce the ${}^7\text{Li} + {}^{58}\text{Ni}$ ADs, the strength of the real SPP should be reduced by $\sim 36\%$. This observed reduction is basically due to the break-up effect of ${}^7\text{Li}$. Second, the extracted (J_V) and (J_W) values from calculations using (real SPP + Imag. WS) approach do present the BTA which agree with the previously reported findings [33,34,37]. ${}^{58}\text{Ni}$ density distributions which were obtained from DHB model [25] as was done in SPP calculations. In other words, both SPP and DF-CDM3Y6 calculations implemented the same densities for ${}^7\text{Li}$ and ${}^{58}\text{Ni}$, so the main difference here was only in the utilized interaction potential. The DF potentials at the different considered energies were generated using DFMSPH code [38]. The real DF potential is prepared by folding the ${}^7\text{Li}$ and ${}^{58}\text{Ni}$ densities with the (V_{NN}).

$$V_{DF}(r) = \iint \rho_p(r_1) \rho_t(r_2) V_{NN}(S) d^3r_1 d^3r_2. \quad (7)$$

TABLE II. Optimal potential parameters for ${}^7\text{Li} + {}^{58}\text{Ni}$ nuclear system using (real SPP + Imag. WS) approach. The values of (J_V), (J_W) and reaction cross sections (σ_R) are displayed.

E (MeV)	N_{RSPP}	χ^2/N	σ_R (mb)	J_V MeV.fm ³	J_W MeV.fm ³
13	0.531	0.01	80.28	223.05	29.99
13.5	0.611	0.02	108.1	256.53	21.93
14.22	0.454	0.61	339.0	190.48	89.71
16.25	0.725	0.64	865.2	303.58	197.36
18.28	0.725	0.24	1129	302.78	188.80
19	0.727	0.94	711.4	303.19	22.18
20.31	0.98	0.62	1361	408.74	185.03
34	0.657	0.8	1818	270.45	89.06
42	0.384	14.2	1815	156.86	61.05

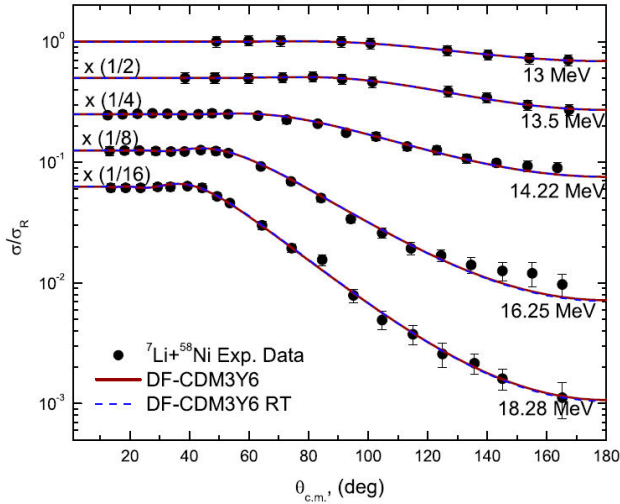


FIGURE 7. Comparison between $^{58}\text{Ni}(^7\text{Li}, ^7\text{Li})^{58}\text{Ni}$ ADs (circles) and calculations using DF Real + DF Imag. (CDM3Y6) approach (solid curves) and CDM3Y6-RT approach (dashed curves) fits at $E_{lab} = 13, 13.5, 14.22, 16.25$ and 18.28 MeV.

The V_{NN} has CDM3Y6 form based on the M3Y-Paris potential and consists of two parts, namely, direct $v_D(s)$ and exchange $v_{EX}(s)$ parts.

$$v_D(s) = \left[11062 \frac{e^{-4s}}{4s} - 2538 \frac{e^{-2.5s}}{2.5s} \right] \text{ MeV}, \quad (8)$$

and the knock-on exchange part in the infinite-range exchange is

$$v_{EX}(s) = \left[-1524 \frac{e^{-4s}}{4s} - 518.8 \frac{e^{-2.5s}}{2.5s} - 7.847 \frac{e^{-0.7072s}}{0.7072s} \right]. \quad (9)$$

The M3Y-Paris interaction is scaled by a density-dependent function $F(\rho)$:

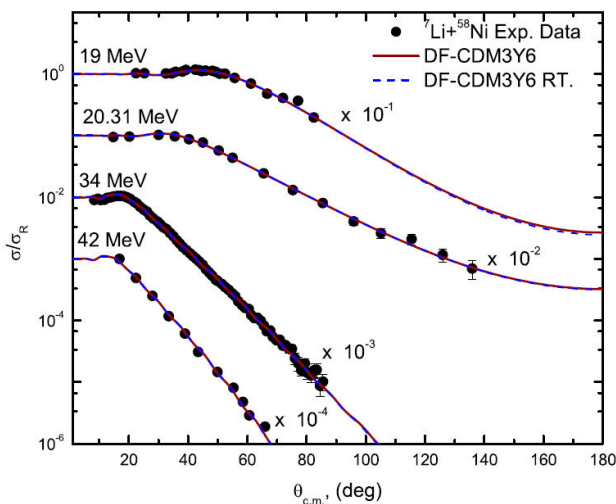


FIGURE 8. Same as Fig. 7 but at $E_{lab} = 19, 20.31, 34,$ and 42 MeV.

$$v_{D(EX)}(\rho, s) = F(\rho)v_{D(EX)}(s), \quad (10)$$

where ρ is the nuclear matter (NM) density, s is the distance between the two interacting nucleons. The $F(\rho)$ function was taken in the following form [39]:

$$F(\rho) = 0.2658[1 + 3.8033 \exp(-1.4099\rho) - 4.0\rho]. \quad (11)$$

So, the nuclear potential has the following form:

$$U(R) = V_C(R) - N_{RDF}V^{DF}(R) - iN_{IDF}V^{DF}(R). \quad (12)$$

The data in this case is fitted by two free parameters N_{RDF} and N_{IDF} , namely, the renormalization factors for the real and imaginary parts of DF potential, respectively.

In addition to the previously described DF calculations using CDM3Y6 interaction, a modified version of CDM3Y6 is employed, which is denoted by CDM3Y6-RT and includes the effect the rearrangement term (RT). In the CDM3Y6-RT interaction, the term $\Delta F(\rho)$ is added and expressed as [40],

$$\Delta F(\rho) = 1.5 [\exp(-0.833\rho) - 1]. \quad (13)$$

The experimental $^7\text{Li} + ^{58}\text{Ni}$ ADs are in a reasonable agreement with the performed calculations using DF-CDM3Y6 potential as shown in Figs. 7 and 8, the extracted optimal N_{RDF} and N_{IDF} values are listed in Table III. The investigation revealed that the real DF potential strength had to be reduced by $\sim 63\%$, the average extracted N_{RDF} value is 0.37 ± 0.17 . Then, we have applied the CDM3Y6-RT approach by considering the impact of including the rearrangement term shown in Eq. (13). Nearly the same quality of fitting was produced as shown in Figs. 7 and 8. The analysis using CDM3Y6-RT confirmed the need to reduce the real DF strength by $\sim 62\%$, where the average extracted N_{RDF} value is 0.38 ± 0.17 . This observed reduction in potential strength is basically due to the break-up effect observed in the weakly bound ^7Li nuclei. The slightly higher N_{RDF} values extracted from the analyses using CDM3Y6-RT approach in comparison with those extracted from CDM3Y6 approach showed that the inclusion of RT has not a significant effect.

3.3. Analysis of $^7\text{Li} + ^{58}\text{Ni}$ data using CFP

Due to the highly clusterization probability of ^7Li and its break-up into $t + \alpha$ at low excitation energy ~ 2.468 , it is interesting to explore the CFP based on the microscopic CFM and to test its applicability to describe the $^7\text{Li} + ^{58}\text{Ni}$ ADs utilizing the following central potential:

$$U(R) = V_C(R) - N_{RCF}V^{CF}(R) - iN_{ICF}W^{CF}(R). \quad (14)$$

In terms of the so called (CFP Real + CFP Imag.) approach, the considered data was reproduced using two varying parameters N_{RCF} and N_{ICF} , namely, the renormalization factors for the real and imaginary CFPs, respectively, generated as defined in Eqs. (3) and (4). Good description for the data

TABLE III. Optimal potential parameters for ${}^7\text{Li} + {}^{58}\text{Ni}$ nuclear system utilizing DF-CDM3Y6 potential with and without RT term. Data are fitted using two parameters namely, N_{RDF} and N_{IDF} . The values of (J_V) , (J_W) and reaction cross sections (σ_R) are displayed.

E (MeV)	Interaction model	N_{RDF}	N_{IDF}	χ^2/N	σ_R (mb)	J_V (MeV.fm ³)	J_W (MeV.fm ³)
13	CDM3Y6	0.237	0.207	0.007	79.79	113.02	98.69
	CDM3Y6-RT	0.247	0.215	0.013	79.58	98.30	85.56
13.5	CDM3Y6	0.283	0.139	0.02	104.9	134.87	66.24
	CDM3Y6-RT	0.295	0.148	0.02	105.1	117.34	58.87
14.22	CDM3Y6	0.2	0.75	0.31	370.4	95.25	357.20
	CDM3Y6-RT	0.2	0.78	0.31	370.5	79.49	310.01
16.25	CDM3Y6	0.504	1.2	0.55	838.7	239.59	570.44
	CDM3Y6-RT	0.512	1.2	0.63	830.7	203.08	475.97
18.28	CDM3Y6	0.517	1.19	0.26	1107	245.31	564.63
	CDM3Y6-RT	0.521	1.19	0.25	1119	206.49	471.64
19	CDM3Y6	0.281	0.104	1.1	727.2	133.24	49.31
	CDM3Y6-RT	0.296	0.115	1.1	729.1	117.09	45.49
20.31	CDM3Y6	0.7	1.04	0.42	1340	331.51	492.53
	CDM3Y6-RT	0.717	1.11	0.42	1343	282.84	437.87
34	CDM3Y6	0.404	0.519	0.81	1834	188.95	242.73
	CDM3Y6-RT	0.427	0.584	0.81	1852	166.53	227.77
42	CDM3Y6	0.222	0.312	23.4	1803	99.59	139.98
	CDM3Y6-RT	0.239	0.363	26.1	1832	88.03	133.70

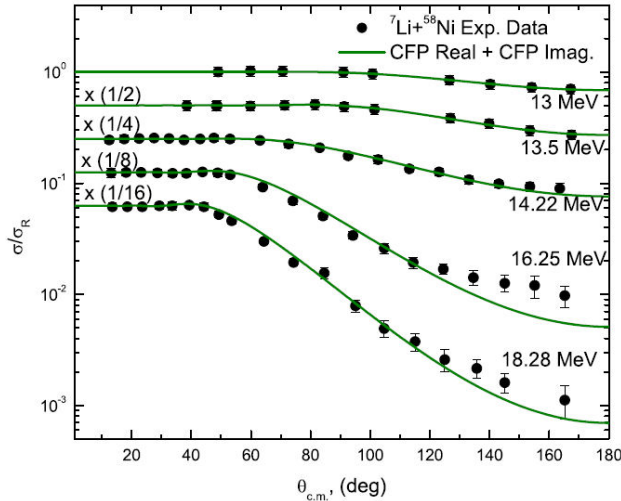


FIGURE 9. Comparison between ${}^{58}\text{Ni}({}^7\text{Li}, {}^7\text{Li}){}^{58}\text{Ni}$ elastic scattering ADs (circles) and OM fits (curves) at $E_{lab} = 13, 13.5, 14.22, 16.25, \text{ and } 18.28$ MeV.

was achieved using CFM at the different considered energies and in the whole angular range as shown in Figs. 9 and 10 except at energies 16.25 and 18.28 MeV which showed a slight deviation at angles $> 120^\circ$. The extracted N_{RCF} value in the energy range 13 – 42 MeV is close to each other with an average value 0.51 ± 0.2 as shown in Table IV. These results confirm the need to reduce the real cluster folding potential strength by $\sim 49\%$ in order to well describe the ${}^7\text{Li} + {}^{58}\text{Ni}$ ADs. This behavior is similar to our findings from the analy-

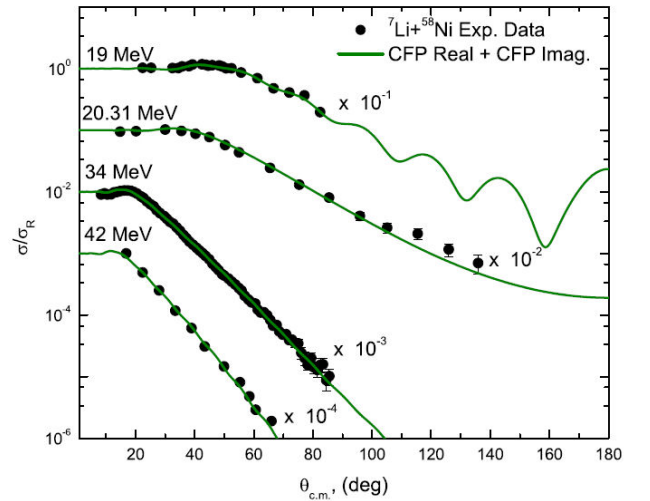


FIGURE 10. Same as Fig. 9 but at $E_{lab} = 19, 20.31, 34, \text{ and } 42$ MeV.

ses using (real SPP + Imag. WS), DF-CDM3Y6 and DF-CDM3Y6 RT approaches. In general, the observed reduction in potential strength is one of the features for systems induced by the weakly bounded ${}^7\text{Li}$ projectile [34].

3.4. Analysis of ${}^7\text{Li} + {}^{58}\text{Ni}$ data using CDCC method

The DF calculations using both CDM3Y6 and CDM3Y6-RT interactions, SPP, and CFP confirmed the need to reduce the real potential strength by $\sim 63\%, 62\%, 36\%, \text{ and } 49\%$, res-

TABLE IV. Optimal potential parameters for ${}^7\text{Li} + {}^{58}\text{Ni}$ nuclear system using (CFP Real + CFP Imag.) approach. The values of σ_R , J_V , and J_W are displayed.

E (MeV)	N_{RCF}	N_{ICF}	χ^2/N	σ_R (mb)	J_V (MeV.fm ³)	J_W (MeV.fm ³)
13	0.458	0.309	0.009	83.98	239.48	31.17
13.5	0.54	0.207	0.02	109.2	282.36	20.874
14.22	0.2	1.178	0.3	387.2	104.58	118.81
16.25	0.749	1.2	2.0	772.8	391.64	121.03
18.28	0.543	1.2	1.1	1012	283.93	121.03
19	0.498	0.19	1.3	744.6	260.40	19.163
20.31	0.839	1.2	1.2	1259	438.70	121.03
34	0.48	1.385	0.77	1962	250.98	139.68
42	0.256	0.96	26.7	1950	133.86	96.82

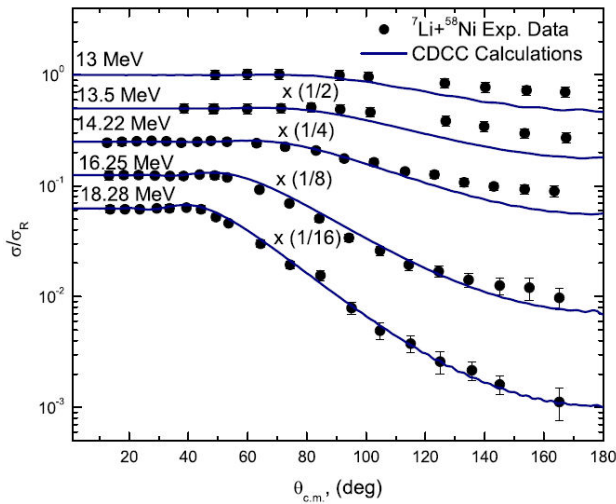


FIGURE 11. Experimental ${}^{58}\text{Ni}({}^7\text{Li}, {}^7\text{Li}){}^{58}\text{Ni}$ ADs (circles) versus CDCC calculations (curves) at $E_{\text{lab}} = 13, 13.5, 14.22, 16.25,$ and 18.28 MeV.

pectively. This observed reduction is mainly due to the effect of ${}^7\text{Li}$ break-up in the field of ${}^{58}\text{Ni}$ target. This effect can be simulated by applying the more sophisticated CDCC method using FRESKO code. The couplings to the unbound $\alpha + t$ resonant and non-resonant continuum states play a significant role as they produce a repulsive real dynamical polarization potential (DPP) [41,42]. The cluster folding (CF) procedures described in Eqs. (3) and (4) are used to calculate the coupling and diagonal potentials. With respect to the momentum of the $\alpha + t$ relative motion, the $\alpha + t$ continuum above the break-up threshold (2.468 MeV) was discretized into a series of momentum bins, with k restricted to $0.0 \leq k \leq 0.75 \text{ fm}^{-1}$ and width $\Delta k = 0.25 \text{ fm}^{-1}$ [43]. The $t + {}^{58}\text{Ni}$, $\alpha + {}^{58}\text{Ni}$, as well as the $\alpha + t$ binding potentials (for $3/2^-$ and $1/2^-$ states) are the same as those used in the performed CFM calculations. As, the most significant contributions come from $L = 3$ resonances [34,43-45], two resonant states ($7/2^-$ and $5/2^-$) with widths of 0.2 and 2.0, respectively, as well as one non-resonant ($1/2^-$, $E_x = 0.4776$ MeV) are included in the CDCC calculations. As shown in Figs. 11 and 12, good

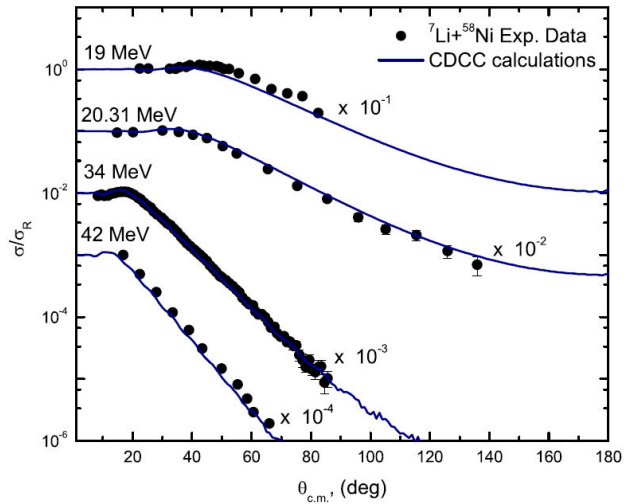


FIGURE 12. Same as Fig. 11 but at $E_{\text{lab}} = 19, 20.31, 34,$ and 42 MeV.

agreement between the experimental ${}^7\text{Li} + {}^{58}\text{Ni}$ ADs and the CDCC calculations was achieved except at the lower energies: 13, 13.5 and 14.22 MeV which exhibited some deviations especially at larger angles $> 100^\circ$, but the over whole agreement is still acceptable as no adjustable parameters were used in the CDCC calculations.

Figure 13 depicts the variation of reaction cross section values obtained for the ${}^7\text{Li} + {}^{58}\text{Ni}$ system by utilizing the OM, SPP, CDM3Y6, CDM3Y6-RT, and CFM potentials as well as those obtained from CDCC calculations with energy at the various examined bombarding energies. The following logarithmic formula can be used to express this behavior:

$$\sigma_R(E) = -637.5 + 70.1E - 0.453E^2. \quad (15)$$

As shown in Fig. 13, there is an observed drop in the value of reaction cross section at 19 MeV. Such drop is presented in the different implemented approaches. The possible explanation of such drop in reaction cross section at $E = 19$ MeV may be due to the presence of resonance

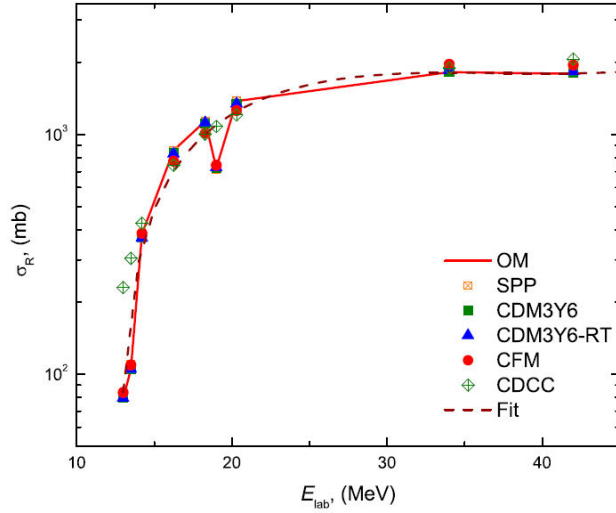


FIGURE 13. Energy versus the extracted σ_R values for ${}^7\text{Li} + {}^{58}\text{Ni}$ system using the different implemented approaches: OM, SPP, CDM3Y6, CDM3Y6-RT, CFM, and CDCC.

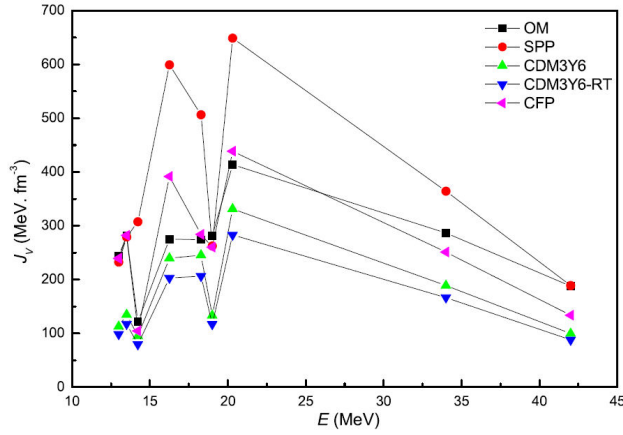


FIGURE 14. Energy dependence on the J_V values obtained from the different implemented approaches.

effect. In order to experimentally justify the presence of this resonance, a study for the excitation function is required. It worth to mention, although the extracted σ_R from CDCC method is quite reasonable (1080 mb), as it agrees well with the neighboring values, but the general agreement between the data and the CDCC calculations at 19 MeV is quite worse than those obtained from the other implemented potentials. Consequently, similar value for σ_R could be obtained from the other implemented approaches if we sacrificed the quality of fitting by reducing the applied constraints on the imaginary part of potential.

The performed analysis within the scope of the various approaches revealed that the BTA phenomenon is well represented in ${}^7\text{Li} + {}^{58}\text{Ni}$ system, as the retrieved J_V values shown in Tables I - IV do not obey the conventional dispersion relation. This is seen in Fig. 14, which depicts the energy dependence on J_V values. Although the retrieved J_V values from the different approaches are significantly differ due to the different methodologies followed in preparing the implemented

nuclear potentials, but the general trend for the variation of J_V values with energy is quite similar.

4. Summary

The weakly bound ${}^7\text{Li}$ nucleus is a good candidate to study the break-up effect on elastic scattering data, as its break-up into $t + \alpha$ cluster structure appears at threshold energy of 2.468 MeV, and has only one bound ($1/2^-$, $E_x = 0.478$ MeV) excited state. From this perspective, it is interesting to explore the mechanism of interaction of weakly projectiles such as ${}^7\text{Li}$ as it also could lead to better understanding for the interaction mechanism of radioactive beams with different targets. The current study aims to reanalyze the available ${}^{58}\text{Ni}({}^7\text{Li}, {}^7\text{Li}){}^{58}\text{Ni}$ ADs at energies 13 – 42 MeV utilizing different interaction potentials:

1. OM calculations with nuclear potential consisting of WS real and imaginary volume parts, and with fixed geometry parameters (radius and diffuseness) were successful in describing the data at the different examined energies.
2. Real SPP + Imag. WS approach, where the considered data was fitted using real SPP and an imaginary part of WS shape with potential parameters fixed to those obtained from OM calculations. One adjustable parameters N_{RSPP} was used to reproduce data. The analysis clarified the need to decrease the real SPP strength by $\sim 36\%$.
3. Double folding potential; using bare CDM3Y6 interaction (DF-CDM3Y6), as well as the inclusion of the rearrangement effect (DF-CDM3Y6 RT) folded into the ${}^7\text{Li}$ and ${}^{58}\text{Ni}$ densities having the same shape as those implemented in SPP calculations. The performed analysis using both CDM3Y6 and CDM3Y6-RT approaches again confirmed the need to decrease the real folded potential strength by ~ 63 and 62% , respectively.
4. Cluster folding potential created based on $t + {}^{58}\text{Ni}$ and $\alpha + {}^{58}\text{Ni}$ potentials at appropriate energies in addition to $t - \alpha$ cluster wave function was employed in the data analysis. The CFM calculations again confirm the need to decrease the strength of the real CFP by $\sim 49\%$ in order to obtain a reasonable fitting.

The reported reduction in potential strength from the different implemented potentials is mainly due to the dissociation of ${}^7\text{Li}$ into $t + \alpha$ in the field of ${}^{58}\text{Ni}$. In order to simulate this effect, coupling to the non-resonant state ($1/2^-$, $E_x = 0.4776$ MeV) and two resonant states ($7/2^-$ and $5/2^-$) with widths of 0.2 and 2.0, respectively, are included in the CDCC calculations. Reasonable fitting for the considered data using the different implemented approaches was obtained. The extracted J_V and J_W values confirm the presence of BTA as they do not obey the usual dispersion relation.

Acknowledgement

This research was funded by the Deanship of Scientific Research at Princess Nourah bint Abdulrahman University, through the Research Funding Program (FRP- 43 -3).

1. P. Amador-Valenzuela, E. F. Aguilera, E. Martinez-Quiroz, D. Lizcano and J. C. Morales-Rivera, Measurements of angular distributions for ${}^7\text{Li}$ elastically scattered from ${}^{58}\text{Ni}$ at energies around the Coulomb barrier *J. of Phys.: Conf. Series* **876** (2017) 012002, <https://doi.org/10.1088/1742-6596/876/1/012002>.
2. K. O. Pfeiffer, E. Speth and K. Bethge, Break-up of ${}^6\text{Li}$ and ${}^7\text{Li}$ on tin and nickel nuclei, *Nucl. Phys. A* **206** (1973) 545, [https://doi.org/10.1016/0375-9474\(73\)90084-5](https://doi.org/10.1016/0375-9474(73)90084-5).
3. T. P. Morrison *et al.*, Coulomb-nuclear interference in the (${}^7\text{Li}$, ${}^7\text{Li}'$) reactions, *J. of Phys. G* **5** (1979) 1751, <https://doi.org/10.1088/0305-4616/5/12/014>.
4. D. W. Glover, R. I. Cutler and K. W. Kemper, Double folding model analysis of ${}^7\text{Li}$ scattering, *Nucl. Phys. A* **341** (1980) 137, [https://doi.org/10.1016/0375-9474\(80\)90366-8](https://doi.org/10.1016/0375-9474(80)90366-8).
5. D. Gupta *et al.*, Breakup of 42 MeV ${}^7\text{Li}$ projectiles in the fields of ${}^{12}\text{C}$ and ${}^{197}\text{Au}$ nuclei *Nucl. Phys. A* **646** (1999) 161, <https://doi.org/10.1007/s12043-001-0177-7>.
6. K. Zerva *et al.*, Quasi-elastic backscattering of ${}^6,{}^7\text{Li}$ on light, medium and heavy targets at near- and sub-barrier energies, *Eur. Phys. J. A* **48** (2012) 102, <https://doi.org/10.1140/epja/i2012-12102-x>.
7. Wen-Di Chenet *et al.*, Microscopic study of ${}^7\text{Li}$ -nucleus potential, *Chinese. Phys. C* **44** (2020) 054109, <https://link.aps.org/doi/10.1088/1674-1137/44/5/054109>.
8. Jin Lei, Inclusive breakup calculations in angular momentum basis: Application to ${}^7\text{Li} + {}^{58}\text{Ni}$ *Phys. Rev. C* **97** (2018) 034628, <https://link.aps.org/doi/10.1103/PhysRevC.97.034628>.
9. A. K. Basak *et al.*, Non-monotonic potentials and vector analyzing powers of ${}^6,{}^7\text{Li}$ scattering by ${}^{12}\text{C}$, ${}^{26}\text{Mg}$, ${}^{58}\text{Ni}$, and ${}^{120}\text{Sn}$, *EPL* **94** (2011) 62002, <https://doi.org/10.1209/0295-5075/94/62002>.
10. M. El-Azab Farid and M.A. Hassanain, Folding model and coupled-channels analysis of ${}^6,{}^7\text{Li}$ elastic and inelastic scattering, *Eur. Phys. J. A* **19** (2004) 231, <https://doi.org/10.1140/epja/i2003-10122-3>.
11. Y. Sakuragi, M. Yahiro, M. Kamimura and M. Tanifuji, Roles of folding spin-orbit potentials in ${}^6,{}^7\text{Li}$ scattering, *Nucl. Phys. A* **462** (1987) 173, [https://doi.org/10.1016/0370-2693\(86\)90696-9](https://doi.org/10.1016/0370-2693(86)90696-9).
12. J. Gomez-Camacho M. Lozano and M.A. Nagarajan, Coupled channel effects in the scattering of ${}^6,{}^7\text{Li}$ BY ${}^{58}\text{Ni}$ *Phys. Lett. B* **161** (1985) 39, [https://doi.org/10.1016/0370-2693\(85\)90604-5](https://doi.org/10.1016/0370-2693(85)90604-5).
13. H. Nishioka, J. A. Tostevin, R. C. Johnson and K. -I. Kubo, Projectile excitation and structure effects in ${}^6\text{Li}$ and ${}^7\text{Li}$ scattering *Nucl. Phys. A* **415** (1984) 230, [https://doi.org/10.1016/0375-9474\(84\)90622-5](https://doi.org/10.1016/0375-9474(84)90622-5).
14. Sh. Hamada and Awad A. Ibraheem, Peculiarities of ${}^6\text{Li}+{}^{12}\text{C}$ elastic scattering, *Int. J. Mod. Phys. E* **28** (2019) 1950108, <https://doi.org/10.1142/S0218301319501088>.
15. Sh. Hamada *et al.*, Analysis of ${}^6\text{Li}+{}^{16}\text{O}$ elastic scattering using different potentials, *Rev. Mex. Fis.* **66** (2020) 322 <https://doi.org/10.31349/RevMexFis.66.322>.
16. Sh. Hamada and Awad A. Ibraheem, Cluster folding optical potential analysis for ${}^6\text{Li}+{}^{28}\text{Si}$ elastic scattering, *Rev. Mex. Fis.* **67** (2021) 276 <https://doi.org/10.31349/RevMexFis.67.276>.
17. Sh. Hamada, Norah A. M. Alsaif and Awad A. Ibraheem, Detailed analysis for ${}^6\text{Li}+{}^{40}\text{Ca}$ elastic scattering using different potentials, *Phys. Scr.* **96** (2021) 055306, <https://doi.org/10.1088/1402-4896/abeba6>.
18. Awad A. Ibraheem *et al.*, Elastic and Inelastic Scattering of ${}^{9,10,11}\text{Be}$ by ${}^{64}\text{Zn}$ and ${}^{120}\text{Sn}$ Nuclei at Different Energies, *Braz. J. Phys.* **51** (2021) 753, <https://doi.org/10.1007/s13538-020-00839-7>.
19. Awad A. Ibraheem, N. A. M. Alsaif, M. Al-Ahmari and Sh. Hamada, Further investigation of ${}^{10,11}\text{B} + {}^{58}\text{Ni}$ elastic scattering, *Phys. Scr.* **96** (2021) 115307 <https://doi.org/10.1088/1402-4896/ac183f>.
20. L. J. Allen, J.P. McTavish, M.W. Kermode and A. McKeerrell, The root-mean-square radius of the deuteron, *J. Phys. G* **7** (1981) 1367, <https://doi.org/10.1088/0305-4616/7/10/014>.
21. G. R. Satchler and W. G. Love, Folding model potentials from realistic interactions for heavy-ion scattering, *phys. Rep.* **55** (1979) 183, [https://doi.org/10.1016/0370-1573\(79\)90081-4](https://doi.org/10.1016/0370-1573(79)90081-4).
22. L. C. Chamon *et al.*, Nonlocal Description of the Nucleus-Nucleus Interaction, *Phys. Rev. Lett.* **79** (1997) 5218, <https://link.aps.org/doi/10.1103/PhysRevLett.79.5218>.
23. L. C. Chamon, D. Pereira, M. S. Hussein, Parameterfree account of quasielastic scattering of stable and radioactive nuclei, *Phys. Rev. C* **58** (1998) 576, <https://link.aps.org/doi/10.1103/PhysRevC.58.576>.
24. L.C. Chamon, The Sao Paulo Potential *Nucl. Phys. A* **787** (2007) 198. <https://doi.org/10.1016/j.nuclphysa.2006.12.032>.
25. B. V. Carlson and D. Hirata, Dirac-Hartree-Bogoliubov approximation for finite nuclei, *Phys. Rev. C* **62** (2000) 054310, <https://link.aps.org/doi/10.1103/PhysRevC.62.054310>.

26. R. A. Hardekopf, R. F. Haglund, Jr., G. G. Ohlsen, W. J. Thompson, and L. R. Veese, Polarized triton elastic scattering at 17 MeV, *Phys. Rev. C* **21** (1980) 906, <https://link.aps.org/doi/10.1103/PhysRevC.21.906>.
27. W. Trombik, K. A. Eberhard, G. Hinderer, H. H. Rossner, A. Weidinger, and J. S. Eck, Back-angle elastic and inelastic scattering of α particles from the even Ni isotopes, *Phys. Rev. C* **9** (1974) 1813 <https://link.aps.org/doi/10.1103/PhysRevC.9.1813>.
28. J. Cook, Global optical-model potentials for the elastic scattering of ${}^{6,7}\text{Li}$ projectiles *Nucl. Phys. A* **388** (1982) 153 [https://doi.org/10.1016/0375-9474\(82\)90513-9](https://doi.org/10.1016/0375-9474(82)90513-9).
29. M. Nassurulla *et al.*, New measurements and analysis of elastic scattering of ${}^{13}\text{C}$ by Be nuclei in a wide energy range, *Eur. Phys. J. A* **57** (2021) <https://doi.org/10.1140/epja/s10050-021-00539-z>.
30. M. Nassurulla *et al.*, New measurements and reanalysis of ${}^{14}\text{N}$ elastic scattering on ${}^{10}\text{B}$ target, *Chinese Phys. C* **44** (2020) 104103, <https://doi.org/10.1088/1674-1137/abab89>.
31. N. Burtebayev *et al.*, Effect of the Transfer Reactions for ${}^{16}\text{O}+{}^{10}\text{B}$ Elastic Scattering, *Acta Phys. Pol. B* **50** (2019) 1, <https://doi.org/10.5506/APhysPolB.50.1423>.
32. Sh. Hamada and Awad A, Ibraheem, Optical model potentials for ${}^{16}\text{O} + {}^{16}\text{O}$ elastic scattering, *Indian J. Phys.* **94** (2020) 87 <https://doi.org/10.1007/s12648-019-01443-5>.
33. V. K. Lukyanov *et al.*, Probing the exotic structure of ${}^8\text{B}$ by its elastic scattering and breakup reaction on nuclear targets, *Eur. Phys. J. A* **53** (2017) 31, <https://doi.org/10.1140/epja/i2017-12222-9>.
34. Sh. Hamada and Awad A. Ibraheem, Anomaly in weakly bound ${}^7\text{Li}$ nucleus in the field of ${}^{208}\text{Pb}$ target, *Int. J. Mod. Phys. E* **31** (2022) 2250019, <https://doi.org/10.1142/S0218301322500197>.
35. I. J. Thompson, Coupled reaction channels calculations in nuclear physics, *Comput. Phys. Rep.* **7** (1988) 167, [https://doi.org/10.1016/0167-7977\(88\)90005-6](https://doi.org/10.1016/0167-7977(88)90005-6).
36. L. C. Chamon, B. V. Carlson and L. R. Gasques, Sao Paulo potential version 2 (SPP2) and Brazilian nuclear potential (BNP), *Comp. Phys. Comm.* **267** (2021) 108061 <https://doi.org/10.1016/j.cpc.2021.108061>.
37. Sh. Hamada and A. A. Ibraheem, Reanalysis of ${}^6\text{Li}+{}^{90}\text{Zr}$ angular distributions using different nuclear potentials, *Journal of Taibah University for Science* **16** (2022) 163, <https://doi.org/10.1080/16583655.2022.2036428>.
38. I. I. Gontchar, M.V. Chushnyakova, A C-code for the double folding interaction potential of two spherical nuclei, *Comput. Phys. Commun.* **181** (2010) 168. <https://doi.org/10.1016/j.cpc.2009.09.007>.
39. Dao T. Khoa, G. R. Satchler, and W. von Oertzen Nuclear incompressibility and density dependent NN interactions in the folding model for nucleus-nucleus potentials, *Phys. Rev. C* **56** (1997) 954 <https://doi.org/10.1103/PhysRevC.56.954>.
40. Dao T. Khoa Nguyen Hoang Phuc, Doan Thi Loan and Bui Minh Loc, Nuclear mean field and double-folding model of the nucleus-nucleus optical potential, *Phys. Rev. C* **94** (2016) 034612. <https://link.aps.org/doi/10.1103/PhysRevC.94.034612>.
41. Yukinori Sakuragi, Masanobu Yahiro, Masayasu Kamimura, Microscopic Coupled-Channels Study of Scattering and Breakup of Light Heavy-Ions, *Prog. Theor. Phys. Suppl.* **89** (1986) 136, <https://doi.org/10.1143/PTPS.89.136>.
42. C. Mahaux, H. Ngo, and G. R. Satchler, Causality and the threshold anomaly of the nucleus-nucleus potential, *Nucl. Phys. A* **449** (1986) 354, [https://doi.org/10.1016/0375-9474\(86\)90009-6](https://doi.org/10.1016/0375-9474(86)90009-6).
43. K. Rusek, J. Gomez-Camacho, I. Martel-Bravo, G. Tungate, Study of polarized ${}^7\text{Li}$ scattering from ${}^{208}\text{Pb}$ at 33 MeV, *Nucl. Phys. A* **614** (1997) 112. [https://doi.org/10.1016/S0375-9474\(96\)00449-6](https://doi.org/10.1016/S0375-9474(96)00449-6).
44. N. Keeley and K. Rusek, Near-barrier polarisation potentials for ${}^{6,7}\text{Li} + {}^{208}\text{Pb}$, *Phys. Lett. B* **427** (1998) 1 [https://doi.org/10.1016/S0370-2693\(98\)00334-7](https://doi.org/10.1016/S0370-2693(98)00334-7).
45. N. Keeley, K. W. Kemper, O. Momotyuk and K. Rusek, ${}^6\text{Li}$ and ${}^6\text{He}$ elastic scattering from ${}^{12}\text{C}$ and the effect of direct reaction couplings, *Phys. Rev. C* **77** (2008) 057601. <https://link.aps.org/doi/10.1103/PhysRevC.77.057601>.